Study of Synthesis Variables in the Nanocrystal Growth Behavior of Tin Oxide Processed by Controlled Hydrolysis

Caue Ribeiro,[†] Eduardo J. H. Lee,[†] Tania R. Giraldi,[†] Elson Longo,[†] José A. Varela,[‡] and Edson R. Leite*,[†]

Universidade Federal de São Carlos, Departamento de Química, Rodovia Washington Luis km 235, 13565-905 São Carlos, SP, Brazil, and Universidade Estadual Paulista "Julio de Mesquita Filho", Instituto de Química, 14801-907 Araraquara, SP, Brazil.

Received: June 17, 2004; In Final Form: July 28, 2004

Tin dioxide nanoparticle suspensions were synthesized at room temperature by the hydrolysis reaction of tin chloride (II) dissolved in ethanol. The effect of the initial tin (II) ion concentration, in the ethanolic solution, on the mean particle size of the nanoparticles was studied. The Sn^{2+} concentration was varied from 0.0025 to 0.1 M, and all other synthesis parameters were kept fixed. Moreover, an investigation of the effect of agglomeration on the nanoparticle characteristics (i.e., size and morphology) was also done by modifying the pH of the SnO_2 suspensions. The different samples were characterized by transmission electron microscopy, optical absorption spectroscopy in the ultraviolet range, and photoluminescence measurements. The results show that higher initial ion concentrations and agglomeration lead to larger nanoparticles. The concentration effect is explained by enhanced growth due to a higher supersaturation of the liquid medium. However, it was observed that the agglomeration of the nanoparticles in suspension induce coarsening by the oriented-attachment mechanism.

1. Introduction

Nanostructured materials have become a topic of increasing interest in past years. This is mainly due to the ability of nanomaterials to display novel or better properties when compared to those of bulk materials,[1−2] which may lead to the development of electronic and optoelectronic nanodevices with superior performance. It is well known that size and morphology are very important parameters in nanostructures. Therefore, it is of fundamental importance to be able to control these aspects and to reproduce them and to control the final properties of the material.[3]

The bottom-up approach, based on chemical routes, has been shown to be a very good alternative to prepare nanomaterials of various systems.[4] A wide variety of chemical methods to obtain nanostructures can be found in the literature. Among them, procedures based on precipitation in liquid environments seem viable to process some types of nanoparticles, such as oxides and sulfides.[3−15] Several of the reported methods are not very easy to execute, with the disadvantages of the use of toxic precursors and the need for precise atmosphere control. However, routes based on the hydrolysis of inorganic precursors are usually simple and less sensitive to atmospheric conditions, and toxicity may be avoided by a proper selection of solvents.

To be able to control and obtain reproducibility in the synthesis of nanoparticles by precipitation in liquid mediums, some processes, such as nucleation, growth, and coarsening, must be more thoroughly understood. Extensive work (e.g., in barium sulfate,[16] calcium oxalate,[17] and calcium carbonate[18]) has been already done in the nucleation and growth of crystals on the millimeter and micrometer scales. On the nanometer scale, much work has been done, especially in metallic (e.g., gold, iron, and copper[1,19]) and semiconductor nanoparticles (e.g., cadmium chalcogenides[3,8−10]). However, investigations of these processes in nanoscaled oxides are scarce. Therefore, it is clear that more studies related to the variables that affect the synthesis of nanoparticles are necessary. Several papers report investigations on the influence of temperature and pressure on the size and shape of nanoparticles, relating these characteristics to coarsening processes, such as the oriented-attachment mechanism,[7,13−15,20−22] and the rate law derived by Lifshift, Slyozov, and Wagner (LSW)[23,24] (i.e., Ostwald ripening). Coarsening mechanisms refer to processes where larger crystals grow at the expense of smaller crystals. These differ from growth mechanisms in the sense that particle growth occurs by the consumption of previously existing particles rather than by the deposition of dissolved ions due to a supersaturation condition.

Synthesis variables in liquid systems have been extensively studied in nanocrystalline TiO_2[5,13−14] and ZnO.[13,15] Recently, there has been a considerable effort to study synthesis procedures for nanocrystalline SnO_2, which is a key functional material that has important applications in gas sensors, solar cells, and doped semiconductors.[1,7] In this sense, a route of importance was reported by Leite et al.[7,25] The process is based on the hydrolysis reaction of tin chloride (II) in an ethanolic solution at room temperature, followed by a dialysis process to cleanse the chloride ions. The final product is a clear suspension of nearly spherical cassiterite nanoparticles, with sizes ranging from 2 to 6 nm. However, synthesis variables in this route have not yet been fully elucidated and optimized.

This work describes an investigation of the effect of the agglomeration and the initial dissolved ion (i.e., Sn^{2+}) concentration on the characteristics of SnO_2 nanoparticles that are synthesized by the route described by Leite et al.[7,25] These variables are not commonly studied in work related to the chemical control of nanoparticle characteristics; however, they should be of great importance because they affect nucleation and growth and coarsening mechanisms. This investigation may

* Corresponding author. E-mail: derl@power.ufscar.br.
[†] Universidade Federal de São Carlos.
[‡] Universidade Estadual Paulista.

10.1021/jp0473669 CCC: $27.50
Published on Web 09/08/2004

give support for a reproducible methodology of synthesis with good particle-characteristics control.

2. Experimental Procedure

The procedure used in this work to obtain nanocrystalline tin dioxide nanoparticles has been described in greater detail elsewhere.[7,25] The synthesis consists of the hydrolysis reaction of $SnCl_2 \cdot 2H_2O$ (Mallinckrodt) in an ethanolic (Merck absolute ethanol) solution at room temperature. The product of this reaction is a white turbid suspension. Dialysis processes in deionized water were carried out to cleanse the chloride ions. The final products are clear colloidal suspensions of nanocrystalline tin dioxide, with a pH of ~8.5. The stability of the suspensions could be observed by the absence of agglomeration on up to 12-month-old samples. X-ray diffraction patterns showed that the final product consists of the cassiterite phase of SnO_2. In this work, the effect of the variation of the initial concentration of Sn^{2+} ions on the characteristics of the resultant nanoparticles was studied. The concentration of tin chloride (II) diluted in ethanol was varied from 0.0025 to 0.1 M.

The investigation of the effect of agglomeration in the nanoparticle characteristics was done by modifying the pH of the original SnO_2 nanoparticle suspension. For this study, suspensions synthesized from a 0.025 M Sn^{2+} ethanolic suspension were used. The initial pH of approximately 8.5 was varied by adding nitric acid (dilute nitric acid, Synth), resulting in a set of samples with pH ranging from 8.5 to 1.5. After 24 h, the samples were redispersed with the addition of the surfactant tetrabutylammonium hydroxide (0.4 M aqueous solution, J. T. Baker) and were sonicated by a ultrasonic probe for 2 min for spectroscopic measurements. The morphology and particle size distribution were characterized by means of a 200-kV transmission electron microscope (Philips CM200). The particle size distribution was estimated by the measurement of at least 200 particles in TEM images. The TEM samples were prepared by wetting carbon-coated copper grids with a drop of the colloidal suspensions for 20 s followed by drying on air. The ζ-potential of the 0.025 M Sn^{2+} suspension was measured in a ζ potential meter (Brookhaven Inst. Corp. Zetaplus). The photoluminescence spectra were collected by a Jobin-Yvon, Inc. fluorolog model FL3-12 fluorimeter. A Xe lamp performed the excitation with the photon wavelength fixed at 250 nm. The PL spectra were collected in the 250−400-nm range with a photomultiplier tube detector. Optical spectra on the ultraviolet and visible light ranges (UV-vis) were collected on Perkin-Elmer equipment in the wavelength range of 220−360 nm. All optical measurements were done on the colloidal suspensions at room temperature. The optical characterization was done to be able to estimate the mean particle radius through a simple physical model. This will be further discussed in greater detail.

3. Results and Discussion

3.1. Effect of the Initial Ion Concentration. Figure 1a shows the absorption spectra of the suspensions that were synthesized from solutions with different Sn^{2+} concentrations (ranging from 0.0025 to 0.1 M). It is possible to observe that there is a dislocation in the absorption spectra for samples with different concentrations. This phenomenon may be related to quantum confinement effects because the size scale is on the order of a few nanometers. The quantum confinement effect can be described as an increase in the effective band-gap energy with a decrease in the particle size for particles with a mean particle size on the order of the exciton Bohr radius. Therefore, the spectra absorption shifts should be dependent on the particle size. The same behavior was observed in the photoluminescence

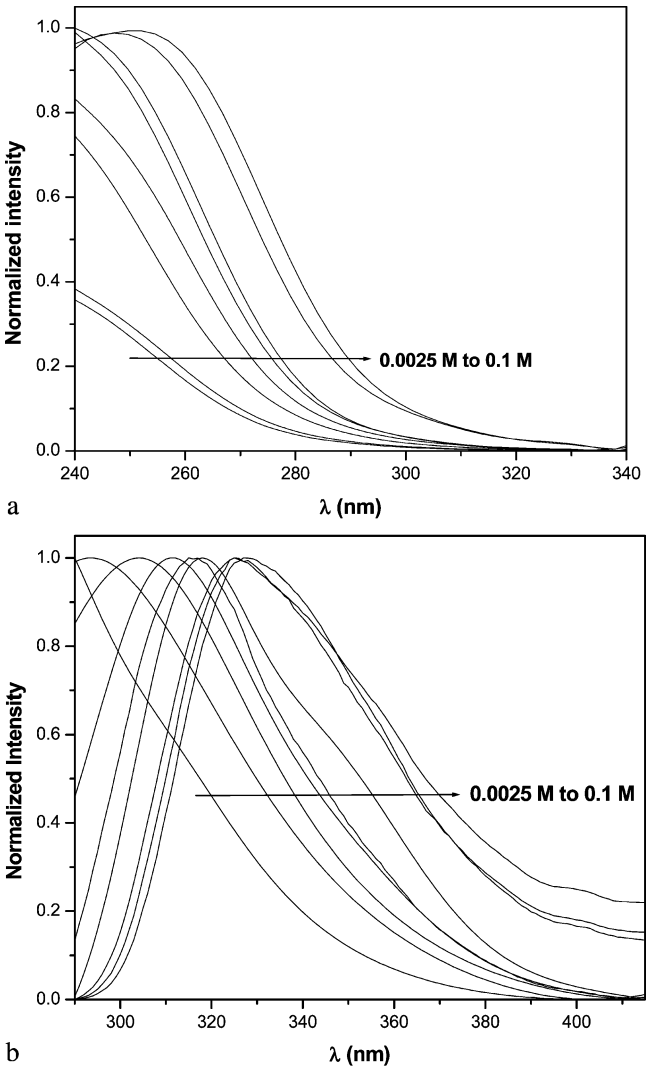

Figure 1. Spectral data for colloidal SnO_2 suspensions synthesized at room temperature with concentrations ranging from 0.0025 to 0.1 M Sn^{2+}. (a) Normalized absorption spectra. (b) Photoluminescence emission spectra.

spectra (PL) shown in Figure 1b. The PL characterization indicates that suspensions with higher concentration of Sn^{2+} ions presented a red shift in the emission peak, indicating that suspensions with higher concentrations of tin ions present particles with a higher mean particle size.

Considering that the position of the emission peak in the PL measurements corresponds to the band-gap energy, it can be observed that all samples present band-gap energies higher than that of bulk SnO_2, which is approximately 3.6 eV. A similar conclusion is reached if the band-gap energy of the samples is considered to be the absorption onset in the optical absorption spectra. The average particle size of the suspensions can be estimated by the blue shift in the band-gap energy through a simple relation derived in the effective mass model[26,27]

$$E_g^{\text{eff}} = E_g + \frac{\hbar^2 \pi^2}{2\mu R^2} \tag{1}$$

where E_g^{eff} is the effective band-gap energy, E_g is the bulk band-gap energy, $\hbar$ is Plank's constant divided by 2π, R is the particle radius, and μ is the effective reduced mass. Lee et al.[28] showed that eq 1 fits the behavior of the effective band-gap energy very well (as calculated from the PL peak position) as a function of particle size (estimated from TEM characterization)

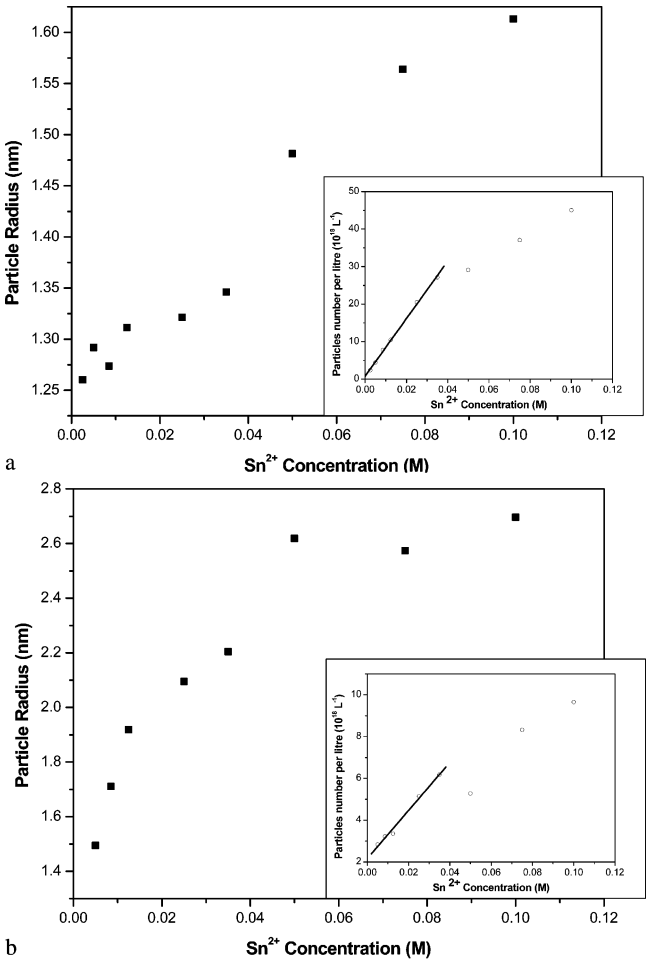

Figure 2. Particle radius vs Sn^{2+} concentration calculated by the effective mass model. (a) Radius estimated by assuming the absorption onset in the UV spectra as band-gap energy. (b) Radius calculated by assuming the PL peak position as band-gap energy.

for the SnO_2 colloidal system. The effective mass model is adequate for particles with a mean radius on the order of the exciton Bohr radius $a_B \approx 2.7$ nm for SnO_2, which is the case for all of the samples prepared in this work.

The band-gap energies that were calculated from the PL curves and the optical absorption spectra are significantly different. As expected, the band-gap energy that was calculated from the absorption onset is higher than the energy calculated from the photon emission. However, because the good agreement between the predictions of the effective mass model and the size dependence of the PL peak position in nanocrystalline SnO_2 particles has already been demonstrated, the estimation of the mean particle radius through eq 1 is considered, in this work, to be more reliable when using the band-gap energy calculated from the PL curves. Figure 2 shows the mean particle radius, estimated from energies calculated from both techniques, plotted as a function of the initial concentration of tin (II) ions. Despite the observed differences, both curves present a linear dependence of the mean particle size as a function of the initial Sn^{2+} concentration for the suspensions with lower initial concentrations. It is well known that the critical radius for a stable nucleus can be calculated by[5]

$$R_c = \frac{2M\bar{\gamma}}{RT\rho \ln\left(\frac{a}{a_0}\right)} \qquad (2)$$

where M is the molecular weight of the precipitated nucleus, $\bar{\gamma}$ is the interfacial energy per area of the formed nucleus, ρ is the density of the material (i.e., 7.02 g/cm^3 for cassiterite), R is the universal gas constant, T is the absolute temperature, a is the mean activity of the substance in solution, and a_o is the saturation activity. The ratio a/a_o is often approximated as c/c_o, that is, the ratio between the mean concentration and the saturation concentration, or supersaturation ratio, S. This last term is dependent only on the concentration. We note that all of the concentration conditions that we have used in this work are above the saturation concentration because precipitation takes place. Moreover, monitoring the synthesis reaction by optical absorption revealed that nucleation is a very fast process. This observation is supported by the fact that for the suspensions synthesized from an initial concentration of 0.0025 M Sn^{2+} the intensity of the absorbance spectra changes only slightly from the initial stages to up to 2 h of monitoring. Because we can associate the intensity of the aborbance spectra with the amount of solids formed, this result indicates that all nucleation and growth from supersaturation occurs in the early stages of the reaction. Therefore, the subsequent particle growth can be ascribed to coarsening mechanisms. Also, a very high water/Sn^{2+} ratio (approximately 500:1) was used, which should promote the acceleration of the hydrolysis reaction. Because nucleation is so fast, we can assume that for the dilute suspensions S is independent of the concentration and, consequently, the mean nuclei size is concentration-independent. Therefore, the differences in the final particle size are related to growth and coarsening processes.

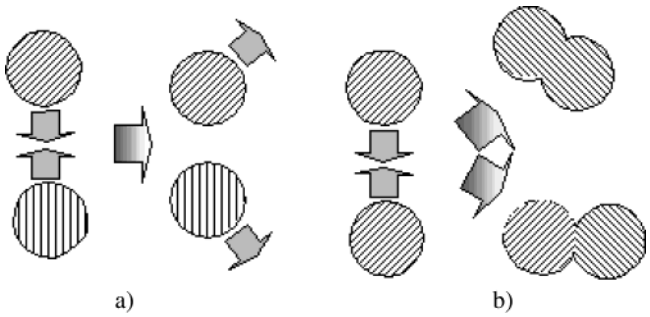

Figure 3. Scheme of the oriented-attachment coarsening mechanism by collisions in colloidal suspensions. (a) Collision in surfaces not crystallographically compatible. Coalescence does not occur. (b) Collision in compatible surfaces. Perfect and imperfect (i.e., coalescence with the formation of defects, such as twin boundaries) oriented attachments are observed.

By considering that coarsening mechanisms are ineffective in dilute suspensions, growth by ion deposition over the surfaces of the nuclei would be the only process that would induce size variation. It is well known for this system that the hydrolysis reaction promotes the formation of $Sn(OH)_4$, which forms SnO_2 by polycondensation. Therefore, the growth of the tin oxide nuclei probably occurs by means of polycondensation reactions rather than by direct ion deposition. The assumption that the growth of the nuclei is the dominant mechanism is reasonable because it is improbable that coarsening by Ostwald ripening is important in this type of system because of the extremely low solubility of SnO_2 at room temperature in ethanol. Moreover, under dilute conditions, coarsening by the oriented-attachment mechanism is not favored because of a reduced interaction between particles. These considerations imply that the final number of nanoparticles would be proportional to the initial concentration. We can estimate the number of particles per liter of suspension by the relation

$$N = \frac{cM}{\rho\alpha R_p^3} \qquad (3)$$

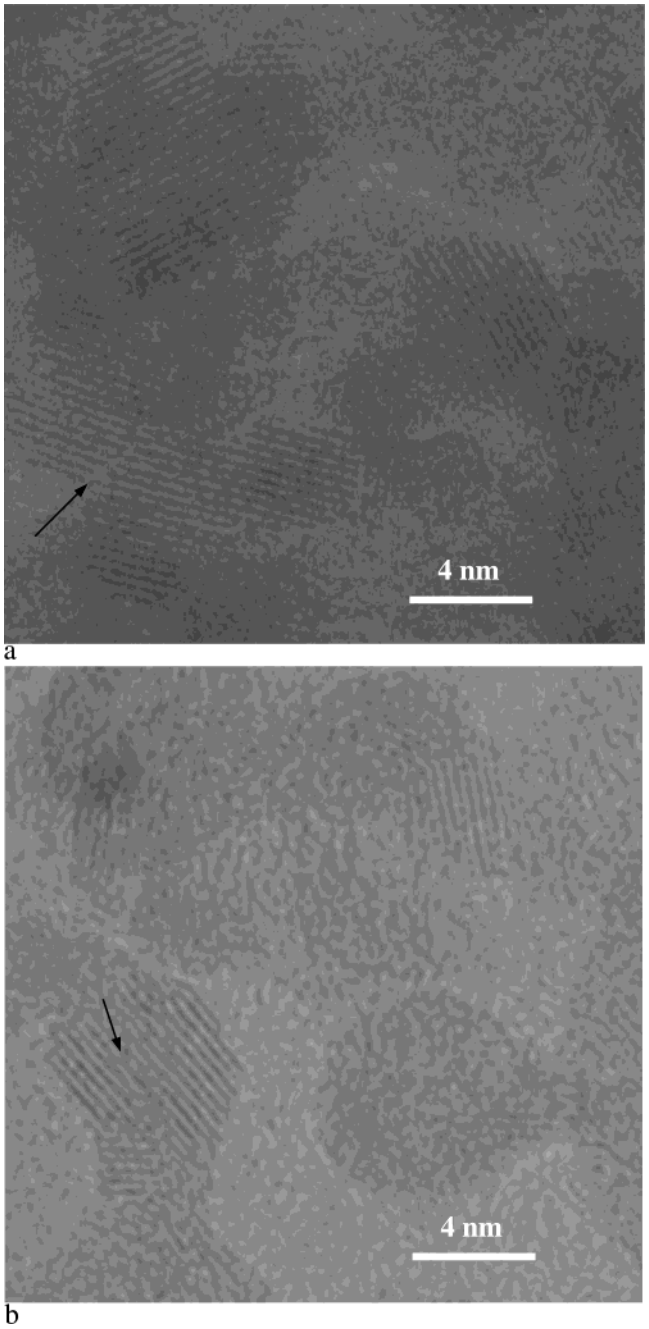

Figure 4. HRTEM images of SnO_2 particles that were obtained from different initial Sn^{2+} concentrations: (a) 0.1 M Sn^{2+} and (b) 0.0025 M Sn^{2+}. The black lines on the images indicate typical defects formed by imperfect coalescence, such as dislocations and twin boundaries.

where c is the initial concentration, R_p is the particle radius, and α is a volumetric shape factor (for a sphere, $\alpha = {}^4/_3\pi$). The inset in Figure 2 shows the calculated number of particles per liter of suspension using R_p as calculated by UV and PL data. In both analyses, a linear concentration dependence of N was observed for suspensions with a c below 0.04 M Sn^{2+}, showing a clear deviation for higher concentrations. An empirical relation between the number of particles and the concentration can be obtained by linear regression using PL data

$$N = (2.16 \pm 0.14) \times 10^{18} + (1.15 \pm 0.07) \times 10^{20} c \quad (4)$$

where N is the number of particles. It is important to observe that the deviation for the suspensions with higher concentrations probably arises when coarsening mechanisms (especially the oriented-attachment process) start to play an important role.

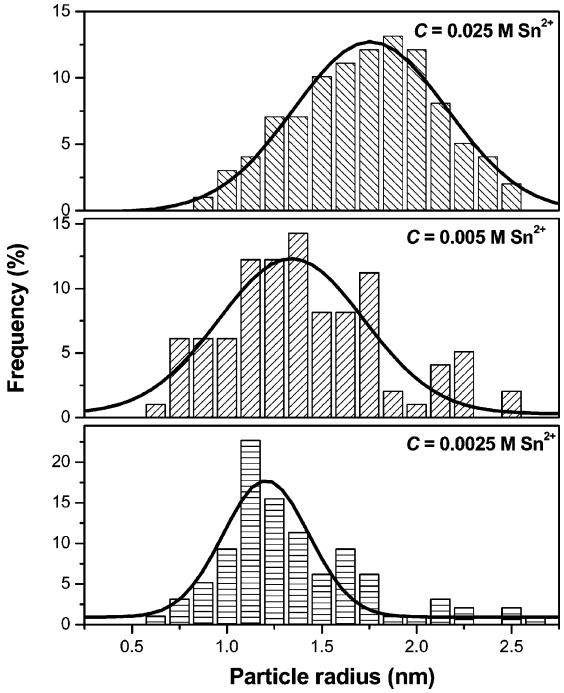

Figure 5. Distribution of SnO_2 particle sizes in colloidal suspensions with initial Sn^{2+} concentrations of 0.0025, 0.005, and 0.025 M.

The oriented-attachment process is believed to occur by a mechanism of crystallographic alignment and coalescence between particles, leading to the formation of a new single crystal. This alignment can be provided by a relative rotation of the particles in contact,[29−31] or it can be statistical, governed by collisions. The last case is possible only in liquid or gas environments, where the degree of freedom of the particles is high. In this case, two kinds of collisions may occur: collisions in different crystallographic orientations, where the coalescence does not occur and the process may be analogous to an elastic collision, and collisions in the same crystallographic orientations, where coalescence occurs and the collision may be describes as inelastic, forming a new single crystal. These hypotheses are exemplified in Figure 3. The collision conditions may be applied to the nanocrystalline system in this work because it is very well dispersed and, at first, no agglomeration effects should have an important role.

Figure 4 shows high-resolution transmission microscopy images (HRTEM) of the suspensions with concentrations of 0.1 (Figure 3a) and 0.0025 M Sn^{2+} (Figure 3b). In the 0.1 M Sn^{2+} suspension, there are several coalesced particles, whereas in the 0.0025 M Sn^{2+} suspension, few are identified. This indicates that under dilute conditions particle collisions can also lead to coalescence. However, suspensions with higher concentrations should present a higher collision frequency, leading to a greater number of coarsened particles. The particle size distributions obtained by direct measurement in TEM images (Figure 5) show that higher concentrations tend to broad distributions, shifting the average size to higher sizes, as expected. The broadening of the size distributions is also typical of the coarsening governed by oriented attachment because the product of the coalescence of two particles is one single-crystalline particle.

3.2. Effect of Particle Agglomeration on the Coarsening of the Nanocrystals. In the case of agglomeration, it is expected that particle coarsening might be favored because of an increase in the collision frequency of particles and to coalescence, which is induced by the rotation of agglomerated particles. To verify this possibility, we investigated the effect of agglomeration

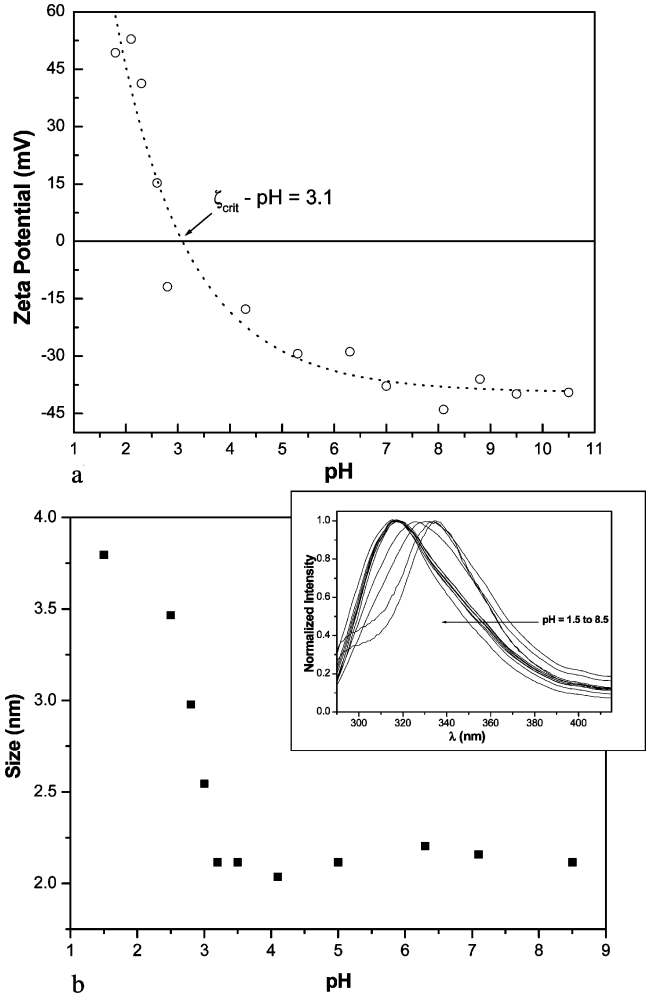

Figure 6. (a) ζ potential vs pH for a SnO_2 colloidal suspension with a 0.025 M initial Sn^{2+} concentration. (b) SnO_2 particle radius vs pH, calculated by PL spectra, for a SnO_2 colloidal suspension with an initial Sn^{2+} concentration 0.025 M. (Inset): Collected PL spectra for suspensions ranging from pH 8.5 to 1.5.

induced by pH modification on the suspensions. The ζ potential of the 0.025 M Sn^{2+} suspension (Figure 6a) shows that there is very high stability against particle agglomeration under nonacidic conditions. The estimated isoelectric point of the suspensions is approximately 3.1. The as-prepared suspensions present a pH of approximately 8.5 and are very stable. By manipulating the pH conditions, it was possible to induce the agglomeration of the nanoparticles. Figure 6b shows the effect of the pH variation on the mean particle size of SnO_2 nanoparticles, as calculated by eq 1 and using the effective band-gap energy from the PL data. The inset in Figure 6b presents the PL curves of the samples with different pH values. It is possible to observe that there is a relation between agglomeration and growth. Significant particle growth was observed for pH values near the isoelectric point. This is expected because in this range of pH agglomeration becomes important and affects growth in two ways: (1) the agglomeration of nanoparticles may lead to a significant increase in collisions during the approximation and (2) particles present in the agglomerated suspension may suffer relative rotations, which might lead to alignments and, consequently, to coalescence. We note that under very acidic conditions the additional growth was on the order of the original particle size, that is, much higher than that observed for the more-concentrated suspensions. Figure 7 shows HRTEM images of samples with different agglomeration conditions (pH values of 6.0 and 2.7). It is clearly observed that the agglomerated

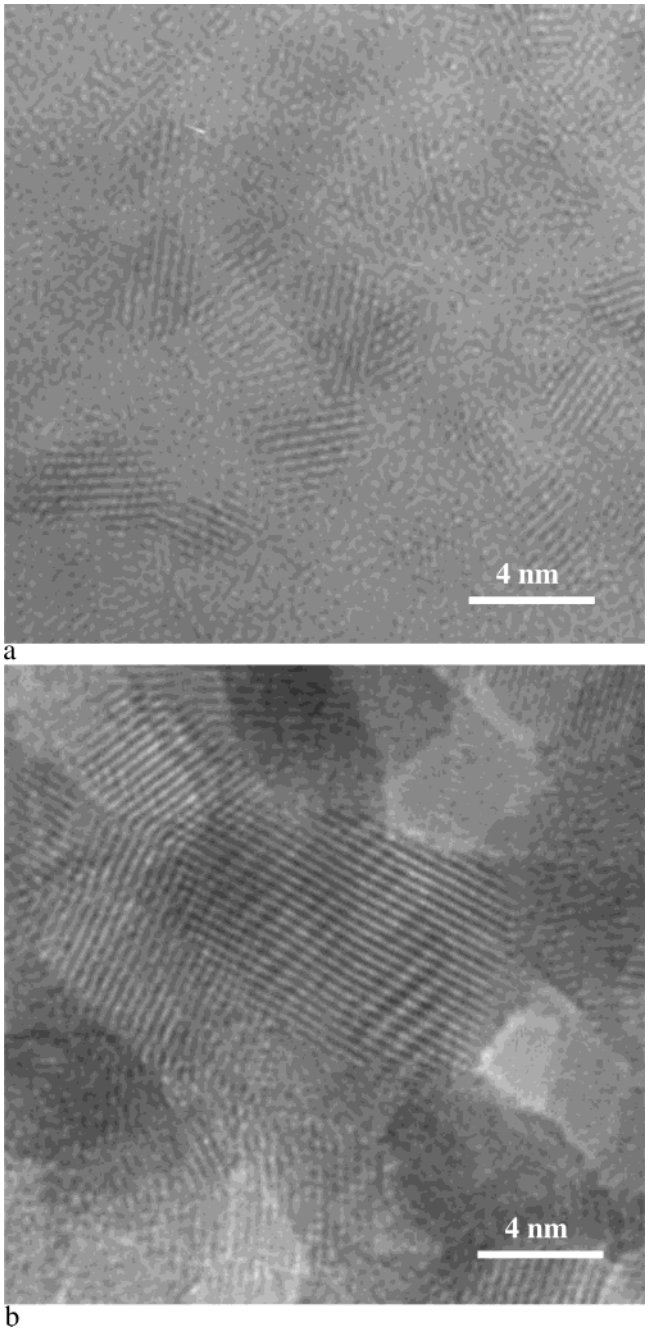

Figure 7. HRTEM images of SnO_2 particles (initial Sn^{2+} concentration 0.025 M) from samples with modified pH values: (a) pH 6.0 and (b) pH 2.7.

suspensions present particles with irregular morphologies and imperfect oriented-attachmentlike defects. Moreover, the particle sizes are much larger than the ones presented by the original 0.025 M Sn^{2+} initial concentration suspensions. However, the aspect of the sample with a pH value of 6.0 is identical to the original 0.025 M Sn^{2+} initial concentration suspensions. This can be explained by the absence of particle coarsening because no agglomeration takes place.

In summary, it was possible to observe that the concentration variation in the synthesis of SnO_2 nanoparticles induces changes in growth and coarsening mechanisms. The growth behavior of the nanoparticles is affected by the differences in the level of supersaturation of the ions in the ethanolic solution. Although coarsening is present in all samples, this process is much more significant in suspensions with high particle concentrations. Therefore, the observed concentration dependence of the mean

particle size is mostly due to growth effects (i.e., deposition of ions over the surface of precipitated nuclei). However, it was possible to observe that agglomeration induces coarsening mechanisms, which lead to significant increases in the mean particle size.

Acknowledgment. We gratefully acknowledge financial support from Brazilian funding agencies FAPESP and CNPq.

References and Notes

(1) Alivisatos, A. P. *J. Phys. Chem.* **1996**, *100*, 13226.
(2) Alivisatos, A. P. *Science* **2000**, *289*, 736.
(3) Peng, X.; Wickham, J.; Alivisatos, A. P. *J. Am. Chem. Soc.* **1998**, *120*, 5343.
(4) Leite, E. R. In *Encyclopedia of Nanoscience and Nanotechnology*; Nalwa, H. S., Ed.; American Scientific: Stevenson Ranch, CA, 2004; Vol. 6, p 537.
(5) Harris, M. T.; Byers, C. H. *J. Non-Cryst. Solids* **1988**, *103*, 49.
(6) Hartel, R. W.; Berlung, K. A. *Mater. Res. Soc. Symp. Proc.* **1986**, *73*, 633.
(7) Leite, E. R.; Giraldi, T. R.; Pontes, F. M.; Longo, E.; Beltrán, A.; Andrés, J. *Appl. Phys. Lett.* **2003**, *83*, 1566.
(8) Hyeon, T.; Lee, S. S.; Park, J.; Chung, Y.; Na, H. B. *J. Am. Chem. Soc.* **2001**, *123*, 12798.
(9) Joo, J.; Na, H. B.; Yu, T.; Yu, J. H.; Kim, Y. W.; Wu, F.; Zhang, J. Z.; Hyeon, T. *J. Am. Chem. Soc.* **2003**, *125*, 11100.
(10) Hyeon, T.; Chung, Y.; Park, J.; Lee, S. S.; Kim, Y. W.; Park, B. H. *J. Phys. Chem. B* **2002**, *106*, 6831.
(11) Boukari, H.; Lin, J. S.; Harris, M. T. *J. Colloid Interface Sci.* **1997**, *194*, 311.
(12) Hu, M. Z. C.; Harris, M. T.; Byers, C. H. *J. Colloid Interface Sci.* **1998**, *198*, 87.
(13) Oskam, G.; Hu, Z.; Lee Penn, R.; Pesika, N.; Searson, P. C. *Phys. Rev. E* **2002**, *66*, 011403−1.
(14) Oskam, G.; Nellore, A.; Lee Penn, R.; Searson, P. C. *J. Phys. Chem B* **2003**, *107*, 1734.
(15) Hu, Z.; Oskam, G.; Lee Penn, R.; Pesika, N.; Searson, P. C. *J. Phys. Chem. B* **2003**, *107*, 3124.
(16) Aoun, M.; Plasari, E.; David, R.; Villermaux, J. *Chem. Eng. Sci.* **1999**, *54*, 1161.
(17) Zauner, R.; Jones, A. G. *Chem. Eng. Sci.* **2000**, *55*, 4219.
(18) Goméz-Morales, J.; Torrent-Burgués, J.; Rodríguez-Clemente, R. *J. Cryst. Growth* **1996**, *169*, 331.
(19) Jensen, P. *Rev. Mod. Phys.* **1999**, *71*, 1695.
(20) Lee Penn, R.; Banfield, J. F. *Science* **1998**, *281*, 969.
(21) Huang, F.; Zhang, H.; Banfield, J. F. *Nano Lett.* **2003**, *3*, 373.
(22) Puntes, V. F.; Krishnan, K. M.; Alivisatos, A. P. *Science* **2001**, *291*, 2115.
(23) Lifshift, I. M.; Slyozov, V. V. *J. Phys. Chem. Solids* **1961**, *19*, 35.
(24) Wagner, C. *Z. Elektrochem.* **1961**, *65*, 581.
(25) Leite, E. R.; Lee, E. J. H.; Giraldi, T. R.; Pontes, F. M.; Longo, E. *J. Nanosci. Nanotechnol.*, in press, 2004.
(26) Gaponenko, S. V. *Optical Properties of Semiconductor Materials*; Cambridge University Press: Cambridge, U.K., 1998.
(27) Brus, L. E. *J. Phys. Chem.* **1986**, *90*, 2555.
(28) Lee, E. J. H.; Ribeiro, C.; Giraldi, T. R.; Longo, E.; Leite, E. R.; Varela, J. A. *Appl. Phys. Lett.* **2004**, *84*, 1745.
(29) Herrmann, G.; Gleiter, H.; Bäro, G. *Acta Metall.* **1976**, *24*, 353.
(30) Moldovan, D.; Yamakov, V.; Wolf, D.; Phillpot, S. R. *Phys. Rev. Lett.* **2002**, *89*, 206101-1.
(31) Haslam, A. J.; Moldovan, D.; Yamakov, V.; Wolf, D.; Phillpot, S. R.; Gleiter, H. *Acta Mater.* **2003**, *51*, 2097.